Supporting Information

Tuning Non-Radiative Decay Channels via Symmetric/Asymmetric Substituent Effects on Phenazine Derivative and Their Phototherapy Switch Between Dynamic and Thermal Process

Yuxuan Li,[a] Keke Ding,[b] Haozhong Wu,[a] Qing Wan,[c] Yao Ma,[a] Yuhua Huang,[b] Zhiming Wang[a], Weijie Zhang*[b], Jianquan Hou*[b], Ben Zhong Tang*[a]*

1. General information

All reagents and solvents were purchased through commercial channels, without secondary purification. Phenazine, sodium hydroxide, sodium hydrosulfite, phosphorus oxychloride, anhydrous magnesium sulfate, malononitrile and ammonium acetate were bought from Energy Chemical Corporation. Bromoethane was purchased from TCI Shanghai Corporation. DSPE-PEG-Mal (M_w = 2,000) was purchased from Laysan Bio Inc. (Arab, AL, U.S.A.). Phosphate-buffered saline (PBS), RPMI 1640 medium (with L-glutamine), fetal bovine serum (FBS), 0.25% Trypsin-EDTA, were obtained from Gibco™ Life Technologies. Penicillin–streptomycin (PEST) solution was purchased from Biosharp (Hefei, China). Cell viability test was measured using the Cell Counting Kit-8 (CCK8, Dojindo, Japan). 2',7'-dichlorodihydrofluorescein diacetate (DCFH-DA) were obtained from Aladdin Co., Ltd. HIV-1 Tat derivant modified with cysteine on C-terminus (RKKRRQRRRC) was customized by Genic Bio (Shanghai, China). The chemical structure of products had been confirmed by nuclear magnetic resonance, high-resolution mass spectrometry, elemental analysis and other analytical methods. ^{1}H and ^{13}C NMR spectra were recorded on a Bruker AV 400/500 spectrometer in DMSO or C_6D_6 at room temperature. High-resolution mass spectra were obtained from Agilent1290 / Bruker maXis impact. Elemental analysis results were measured by Vario EL cube. The UV-vis spectra and PL spectra were carried out by a Shimadzu UV-2600 spectrophotometer and Horiba Fluoromax-4 spectrofluorometer. The absolute fluorescence quantum efficiency was recorded on Hamamatsu absolute PL quantum yield spectrometer C11347 Quantaurus_QY. Electron paramagnetic resonance spectra were conducted on a Bruker ELEXSYS II. The Confocal laser

scanning microscopy images was obtained by LSM 880 confocal laser scanning microscope.

2. Synthetic route

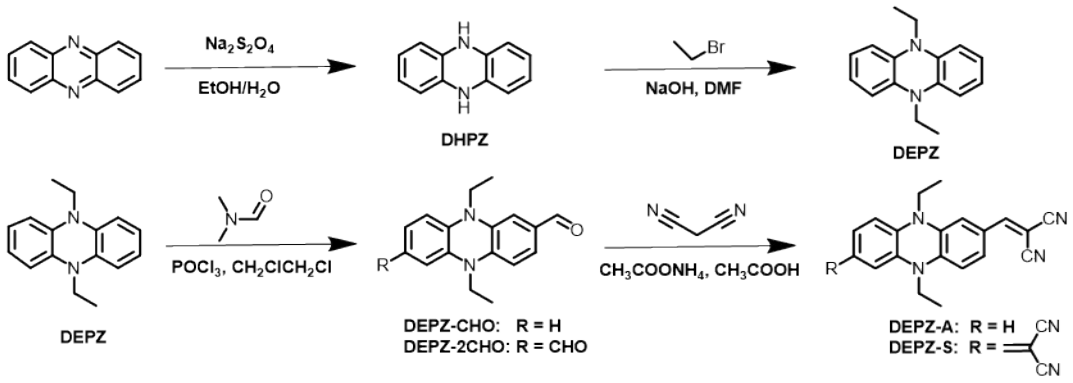

Fig. S1 The synthesis routes of DEPZ-S and DEPZ-A

3. Additional data

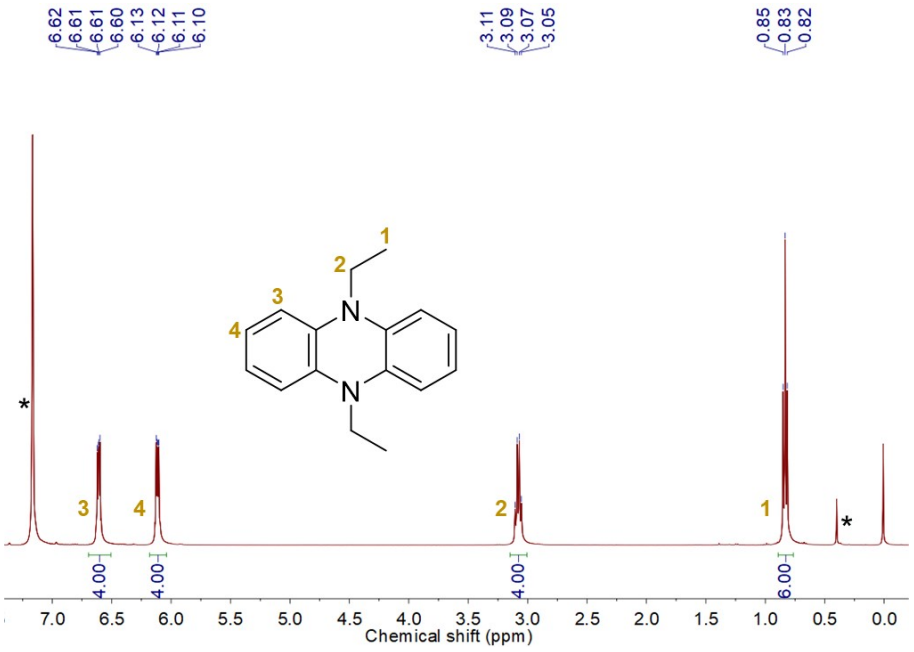

Fig. S2 ^{1}H NMR spectrum of DEPZ in C_6D_6 at 298K.

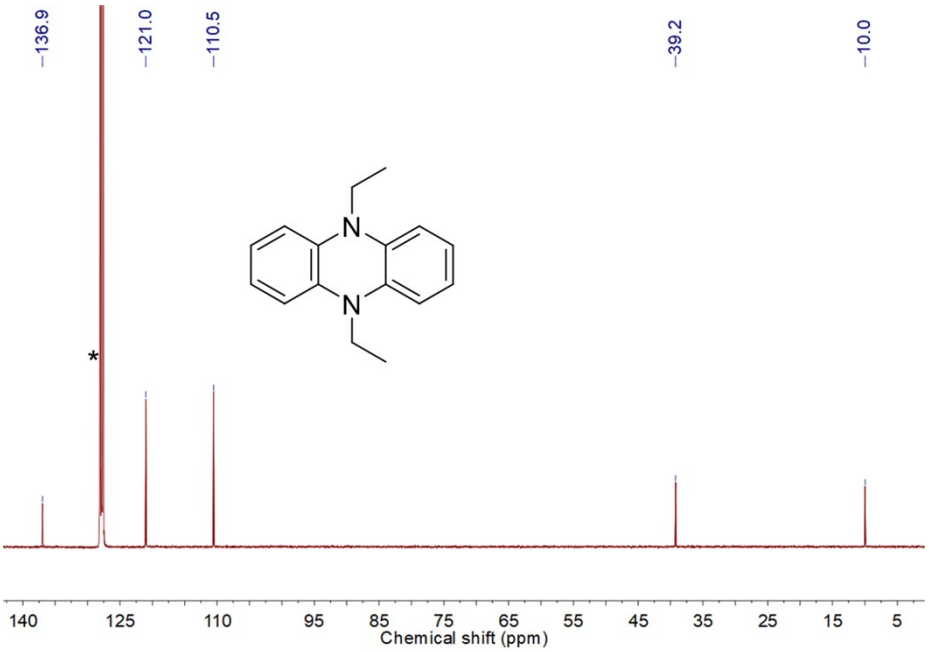

Fig. S3 ^{13}C NMR spectrum of DEPZ in C_6D_6 at 298K.

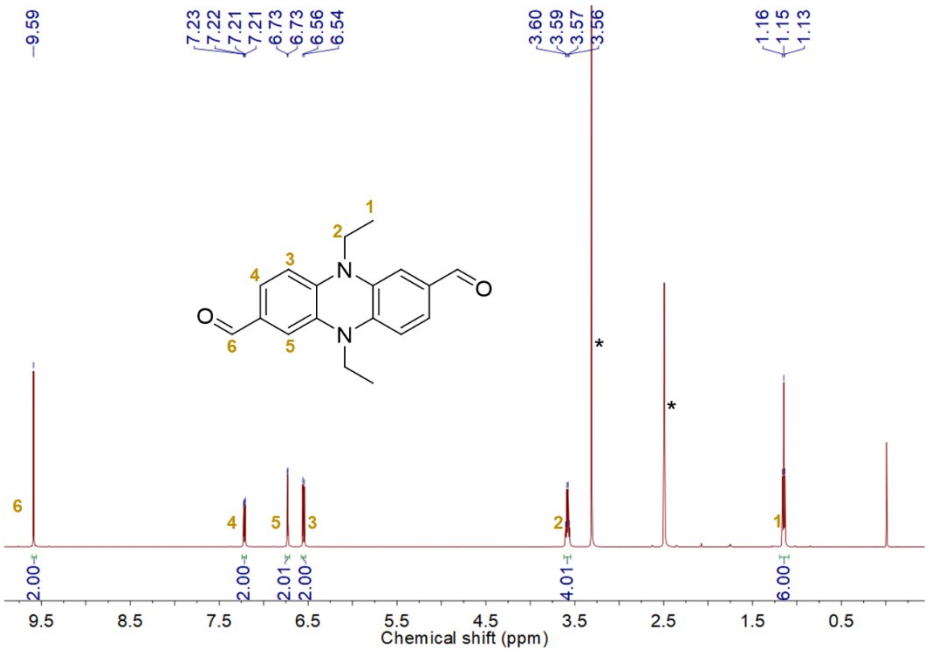

Fig. S4 ^{1}H NMR spectrum of DEPZ-2CHO in DMSO at 298K.

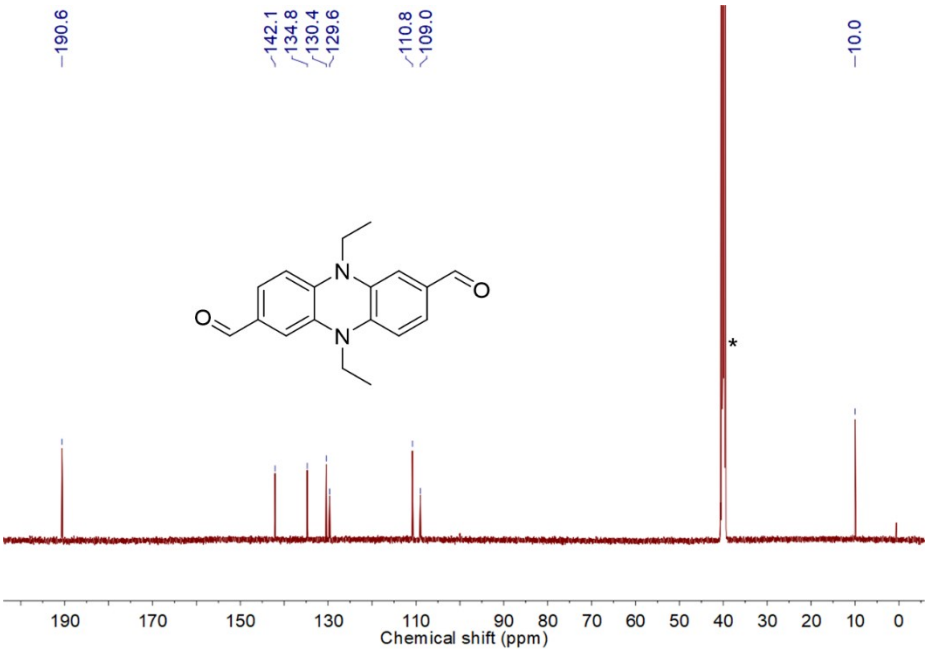

Fig. S5 ^{13}C NMR spectrum of DEPZ-2CHO in DMSO at 298K.

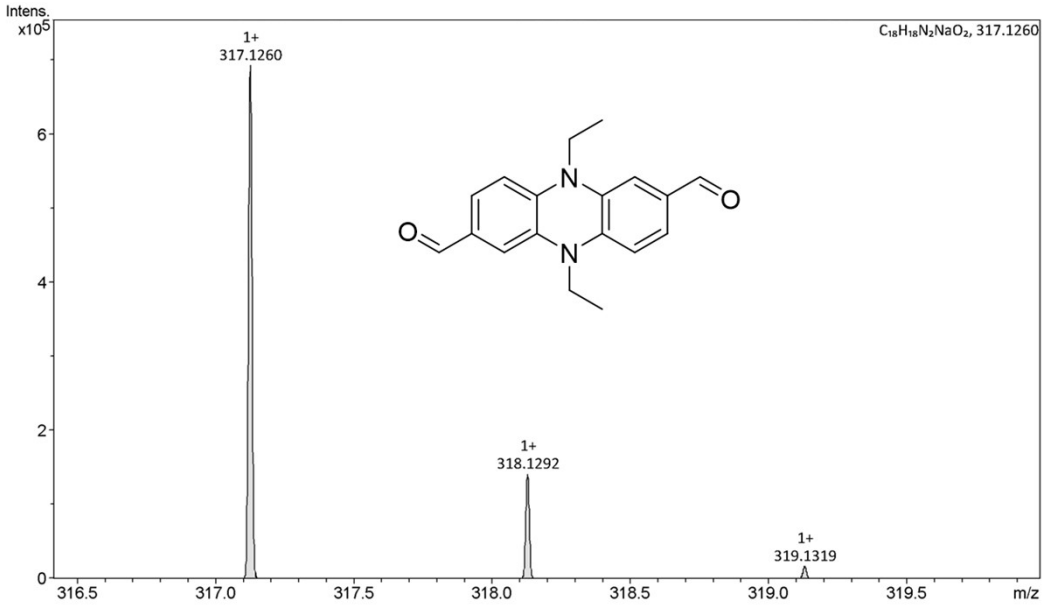

Fig. S6 HRMS spectrum of DEPZ-2CHO.

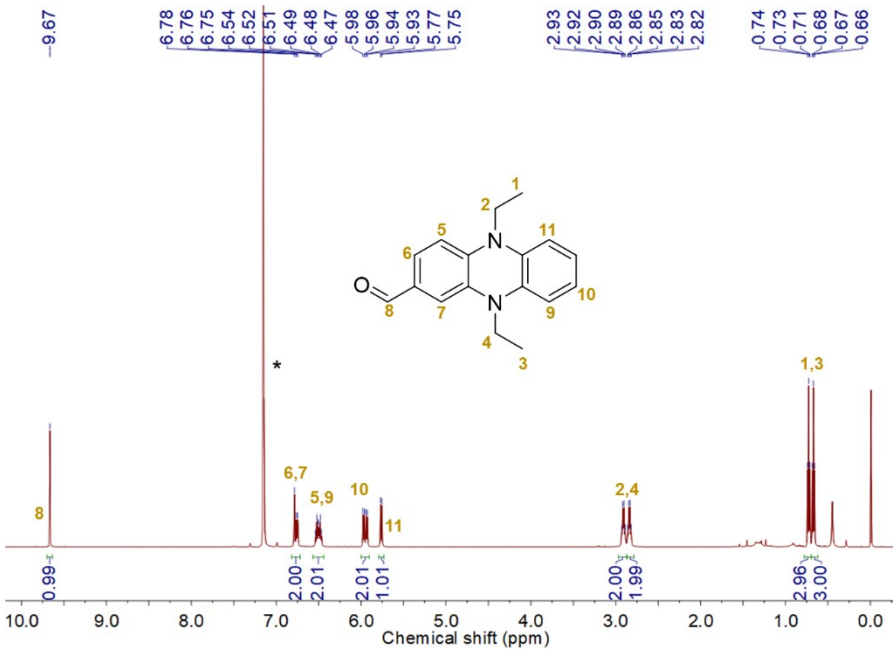

Fig. S7 ^{1}H NMR spectrum of DEPZ-CHO in C_6D_6 at 298K.

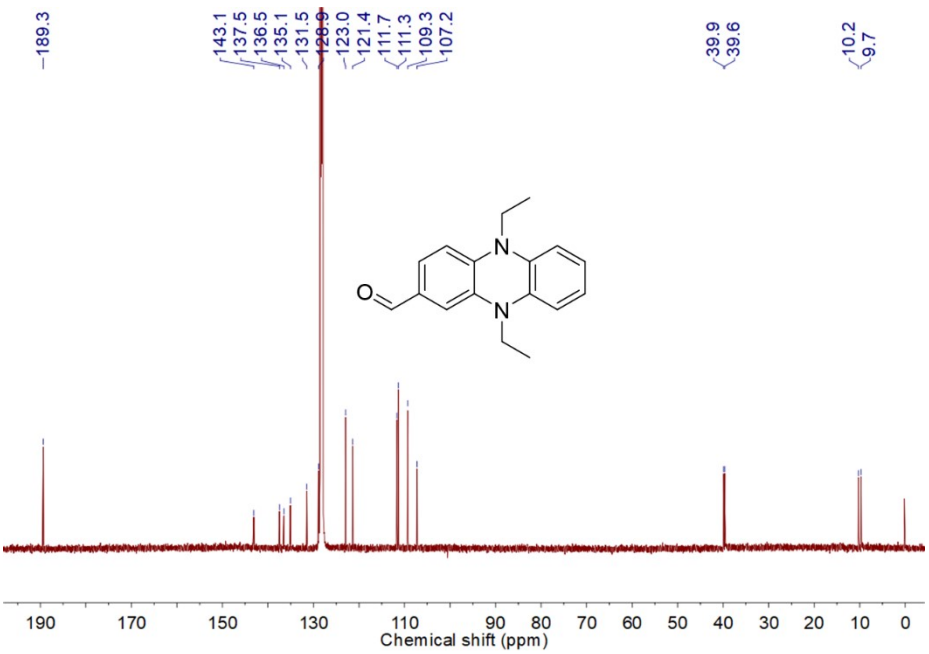

Fig. S8 ^{13}C NMR spectrum of DEPZ-CHO in C_6D_6 at 298K.

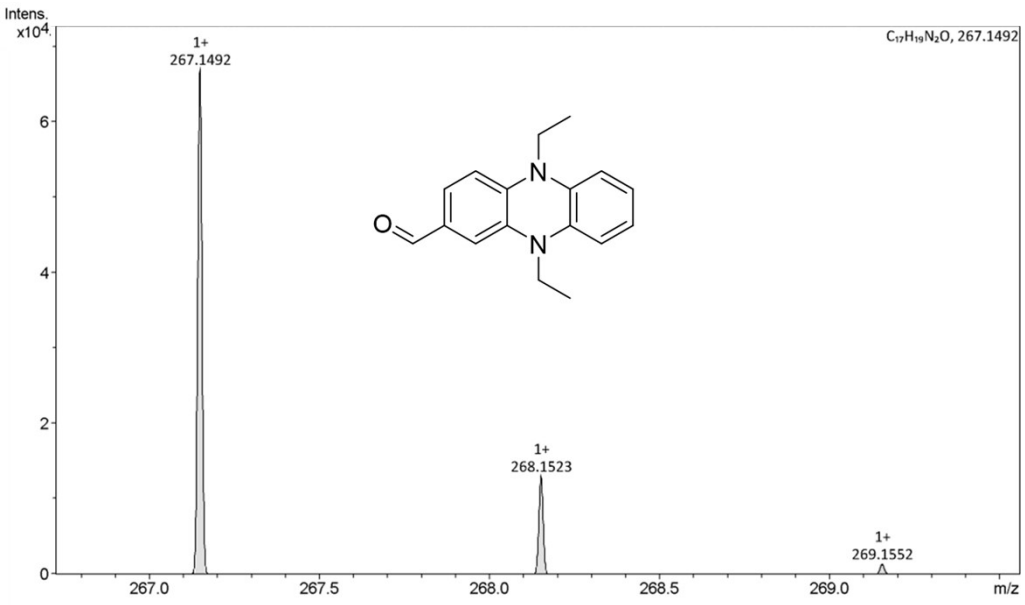

Fig. S9 HRMS spectrum of DEPZ-CHO.

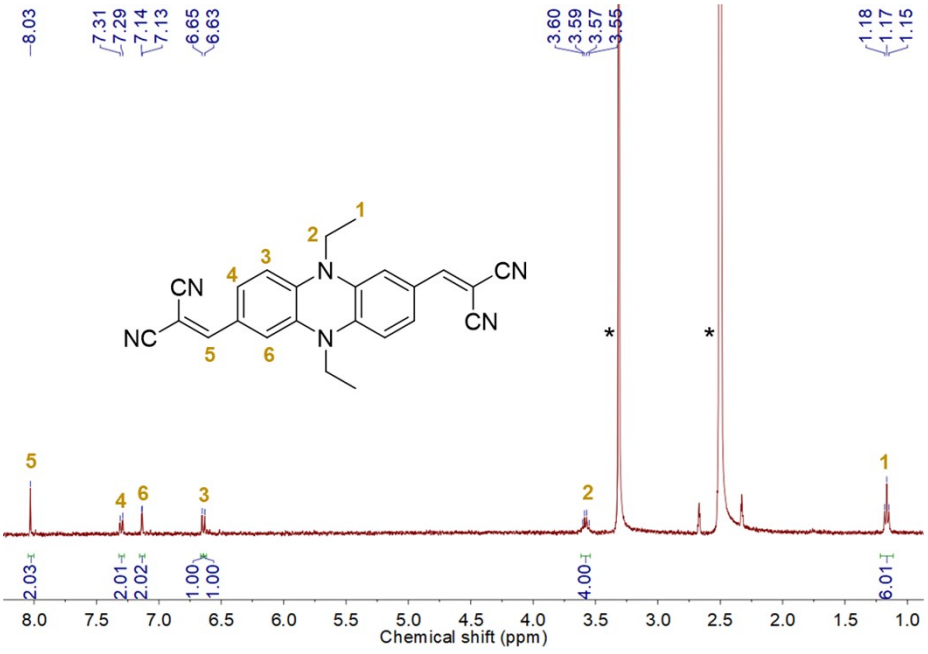

Fig. S10 ^{1}H NMR spectrum of DEPZ-S in DMSO at 298K.

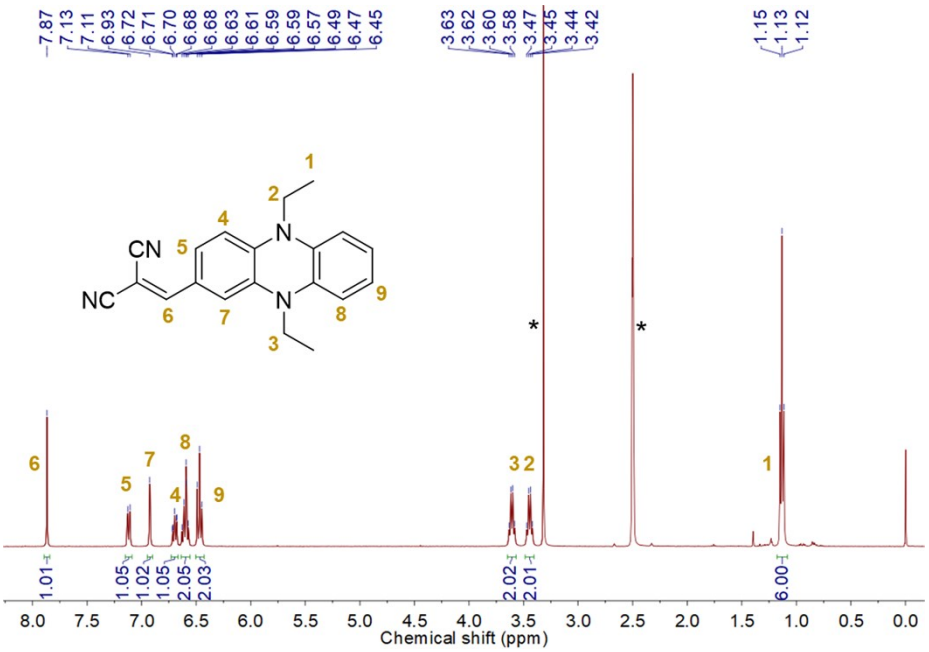

Fig. S11 ^{1}H NMR spectrum of DEPZ-A in DMSO at 298K.

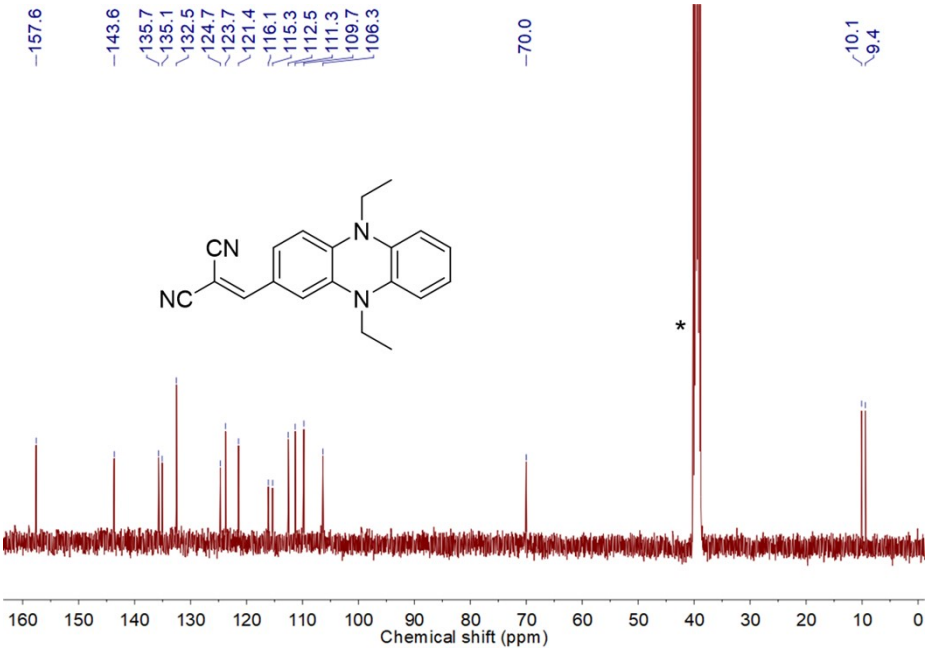

Fig. S12 ^{13}C NMR spectrum of DEPZ-A in DMSO at 298K.

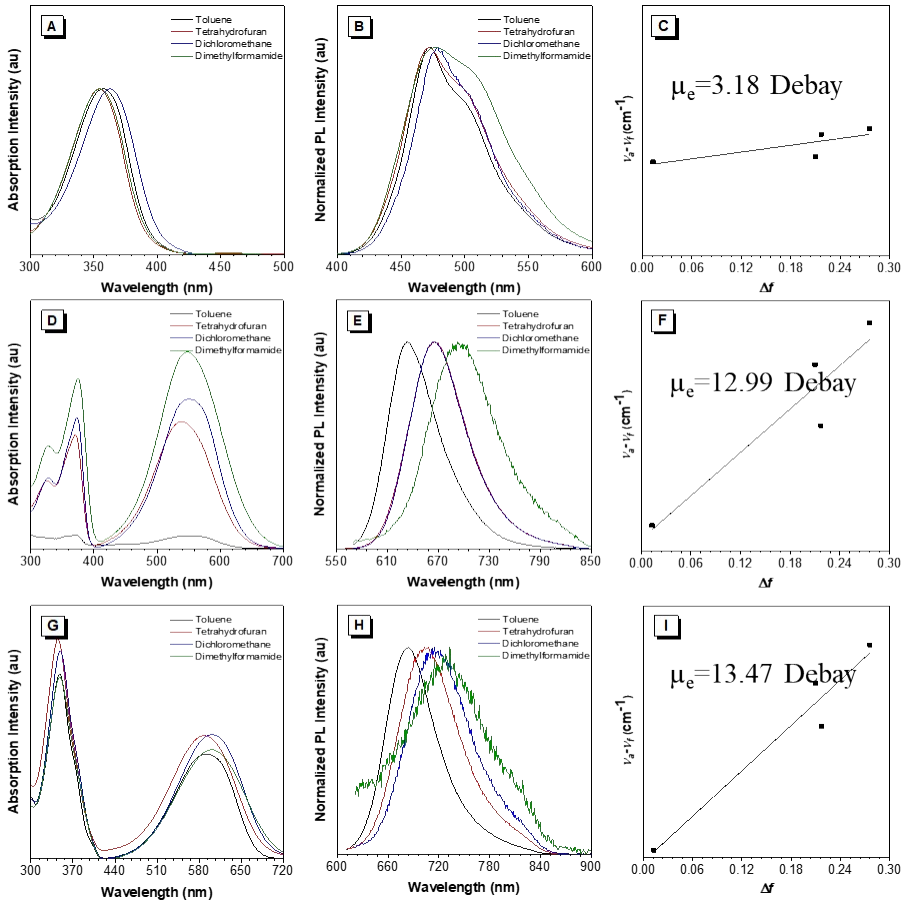

Fig. S13 Solvatochromic absorption spectra of (A) DEPZ, (D) DEPZ-S and (G) DEPZ-A; Solvatochromic PL spectra of (B) DEPZ, (E) DEPZ-S and (H) DEPZ-A; Solvatochromic Lippert-Mataga models of (C) DEPZ, (F) DEPZ-S and (I) DEPZ-A, concentration: 10 μM.

Table 1. Detailed data of DEPZ in different solvents.

Solvents	ε	n	$f(\varepsilon,n)$	λ_{abs} [a)] [nm]	λ_{em} [b)] [nm]	Stokes shift [cm^{-1}]
Toluene	2.38	1.496	0.013	358	472	6747
Tetrahydrofuran	7.58	1.407	0.210	358	472	6791
Dichloromethane	8.93	1.424	0.217	358	476	6969
Dimethyl Formamide	37.00	1.427	0.276	358	478	7012

[a)]Maximum absorption wavelength; [b)]Maximum emission wavelength, concentration: 10 μM

Table 2. Detailed data of DEPZ-S in different solvents.

Solvents	ε	n	$f(\varepsilon,n)$	λ_{abs} [a)] [nm]	λ_{em} [b)] [nm]	Stokes shift [cm^{-1}]
Toluene	2.38	1.496	0.013	551	633	2351
Tetrahydrofuran	7.58	1.407	0.210	538	665	3550
Dichloromethane	8.93	1.424	0.217	553	665	3046
Dimethyl Formamide	37.00	1.427	0.276	546	696	3947

[a)]Maximum absorption wavelength; [b)]Maximum emission wavelength, concentration: 10 μM

Table 3. Detailed data of DEPZ-A in different solvents.

Solvents	ε	n	$f(\varepsilon,n)$	λ_{abs} [a)] [nm]	λ_{em} [b)] [nm]	Stokes shift [cm^{-1}]
Toluene	2.38	1.496	0.013	593	683	2222
Tetrahydrofuran	7.58	1.407	0.210	589	704	2773
Dichloromethane	8.93	1.424	0.217	600	715	2681
Dimethyl Formamide	37.00	1.427	0.276	602	728	2875

[a)]Maximum absorption wavelength; [b)]Maximum emission wavelength, concentration: 10 μM.

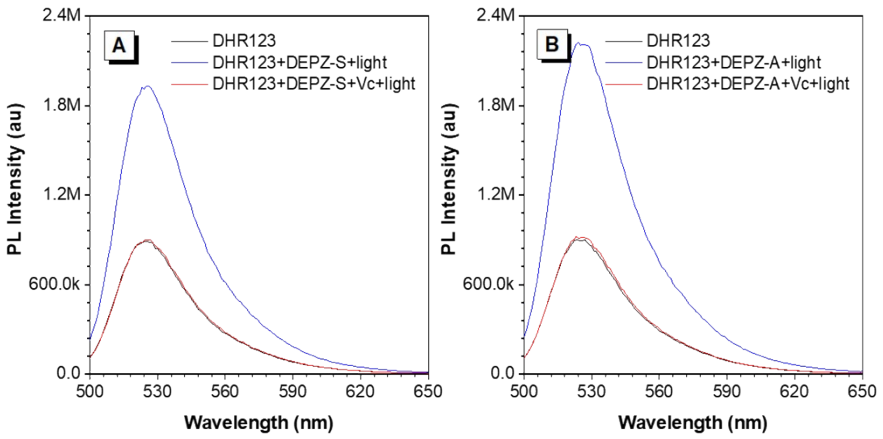

Fig. S14 Time-dependent changes of PL intensities for DHR123 (10 μM) with Vc (10 μM), (A) DEPZ-S (10 μM), (B) DEPZ-A (10 μM) in DMSO/PBS (v/v=1:9).

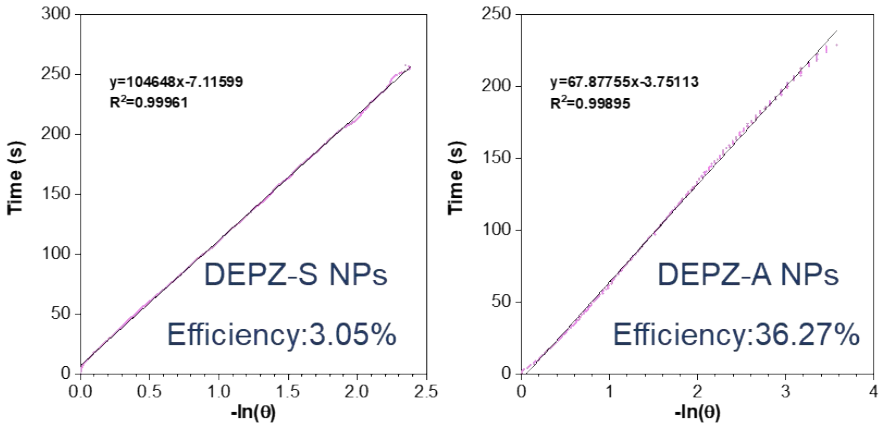

Fig. S15 The linear fitting of time the cooling period vs. negative natural logarithm of driving force temperature for DEPZ-S NPs and DEPZ-A NPs.

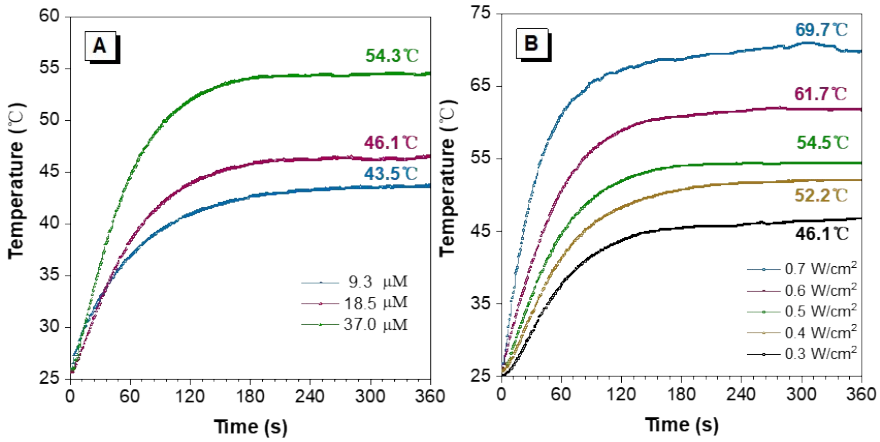

Fig. S16 (A) Photothermal curves of DEPZ-A nanoparticles at different concentrations under 660 nm laser (0.5 W/cm^2) for 6 min. (B) Photothermal curves of DEPZ-A nanoparticles irradiated by 660 nm laser of different power density gradients for 6 min, concentration: 37 μM.

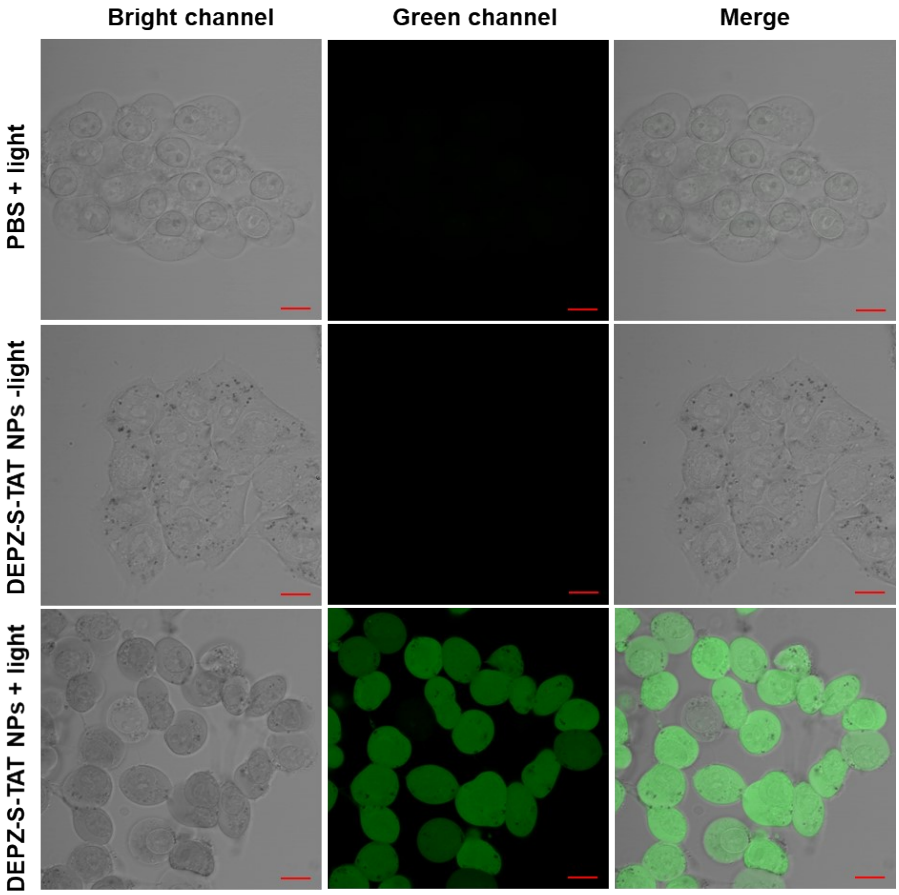

Fig. S17 CLSM images of intracellular ROS in MB49 cells using H2DCFH-DA with DEPZ-S-TAT nanoparticles (32 μM) upon diverse treatments. Scale bar: 10 μm.